Eur. Phys. J. D **20**, 45–54 (2002)
DOI: 10.1140/epjd/e2002-00122-3

THE EUROPEAN PHYSICAL JOURNAL D

Dynamics of a single ion in a perturbed Penning trap. Sextupolar perturbation

J.P. Salas[1,a], M. Iñarrea[1], and A.I. Pascual[2]

[1] Area de Física Aplicada, Universidad de La Rioja, Edificio Científico Tecnológico, C/Madre de Dios 51, 26006 Logroño, Spain
[2] Departamento de Matemáticas y Computación, Universidad de La Rioja, C/Luis de Ulloa s/n, 26004 Logroño, Spain

Received 6 September 2001 / Received in final form 19 March 2002
Published online 28 June 2002 –

Abstract. In the frame work of classical mechanics, we study the nonlinear dynamics of a single ion trapped in a Penning trap perturbed by an electrostatic sextupolar perturbation. The perturbation is caused by a deformation in the configuration of the electrodes. By using a Hamiltonian formulation, we obtain that the system is governed by three parameters: the z-component of the canonical angular momentum P_ϕ – which is a constant of the motion because the perturbation we assume is axial-symmetric –, the parameter δ that determines the ratio between the axial and the cyclotron frequencies, and the parameter a which indicates how far from the ideal design the electrodes are. We study the case $P_\phi = 0$. By means of surfaces of section, we show that the phase space structure is made of three fundamental families of orbits: *arch*, *loop* and *box* orbits. The coexistence of these kinds of orbits depends on the parameter δ. The escape is also explained on the basis of the shape of the potential energy surface as well as of the phase space structure.

PACS. 05.45.-a Nonlinear dynamics and nonlinear dynamical systems – 39.10.+j Atomic and molecular beam sources and techniques – 52.25.Gj Fluctuation and chaos phenomena

1 Introduction

One of the most useful devices in atomic physics for trapping charged particles is the Penning trap [1]. Because charged particles can be confined in a Penning trap for a long time, experiments have led, among other things, to very precise spectroscopic measurements [2], Coulomb crystal studies [3] and accurate atomic clocks [4]. Moreover, as Cirac and Zoller [5] introduced for the first time, one of the most important applications of ion traps today is in quantum computing. In this sense, experimentalists are able to manipulate the quantum information stored in an array of trapped ions by using laser pulses [6]. In particular, the idea of Marzoli and Tombesi [7] of using electrons as trapped particles for quantum computation is very promising. For a general review of the state of the art of ion trapping, we refer the reader to [8].

Besides the above cited features, Penning traps proved to be a very useful theoretical and experimental tool for studying nonlinear collective phenomena in classical and quantum mechanics (see *e.g.* [9] and references therein). When we are dealing with a perfect Penning trap, the motion of the non interacting trapped ions remains harmonic. However, as it was studied by several authors [10–13], electrostatic field perturbations may arise from imperfections in the physical design of the electrodes as well as from misalignments in the experimental mounting. We can separate these perturbations in two groups: harmonic and anharmonic perturbations. In particular, the second group is the most interesting because it leads to nonlinear motion.

A starting point to study the classical nonlinear dynamics of perturbed Penning traps is to consider a single trapped ion. This possibility was also pointed out by Bergeman for a single cooled atom trapped in a Quadrupole Magnetostatic Trap [14]. As we will see in the next section, a general theoretical study of the motion of a single ion in a perturbed Penning trap is an almost impossible task. Hence, in this paper we only consider axially-symmetric perturbations of the three-dimensional Penning trap, which is also axially-symmetric. In particular, we will treat the *sextupolar* perturbation and, following previous works on perturbed Rydberg atoms under external fields [15], the study is performed from a numerical point of view by using Poincaré surfaces of section.

At this point, we remark that, although electrostatic perturbations are usually undesirable, they may be experimentally added by modifying the electrostatics of the trap. Theoretical works along this line were done by Backhaus *et al.* [16]. An alternative to these kinds of perturbed traps, based on a combined Penning-Ioffe trap, has been recently suggested [17].

The paper is organized as follows. Section 2 is devoted to the posing of the problem. A general model for the

[a] e-mail: josepablo.salas@dq.unirioja.es

nonlinear electrostatic imperfections is assumed. In order to manage a two-degrees of freedom system, we assume that only axial-symmetric electrostatic perturbations take place. Moreover, among all the axial-symmetric nonlinear terms appearing in the model, we only consider the axial-symmetric sextupolar one. The corresponding Hamiltonian for a single ion is established, and the relevant parameters controlling the dynamics are determined. Section 3 is dedicated to analyzing the effective potential energy surface appearing in the Hamiltonian. From this study, we can understand part of the dynamics. In Section 4, we find the fundamental families of orbits that determine the phase space structure by using Poincaré surfaces of section. Special attention is paid to three points: the stability of the fixed points appearing in the surfaces of section, the bifurcation between them, and the ion escape mechanics. Finally, in Section 5 we present a discussion of the results.

2 The perturbed Penning trap

The Penning trap provides three-dimensional trapping by means of an axially-symmetric ("*perfect*") quadrupole electric field plus a static homogeneous magnetic field along the z-direction. The perfect electric quadrupole potential is achieved by means of a set of three electrodes. These electrodes are infinite hyperboloids of revolution whose equations are

$$\frac{\rho^2}{\rho_0^2} - \frac{z^2}{z_0^2} = \pm 1, \qquad \rho^2 = x^2 + y^2. \tag{1}$$

The minus sign in (1) stands for the electrode called the *ring*, while the plus sign refers to the other two electrodes called *end-cap* placed above and below the ring. The constants ρ_0 and z_0 are, respectively, the inner radius of the ring electrode and half the distance between the two end-caps, and they are related through $\rho_0^2 = 2z_0^2$. A voltage U_0 is applied to the end-cap electrodes with respect to the ring. In this configuration, a single ion of mass m and charge q is subjected to a electrostatic quadrupole potential given by

$$V(x,y,z) = \frac{mw_z^2}{4q}(2z^2 - x^2 - y^2), \tag{2}$$

where $w_z = (4qU_0/mR_0^2)^{1/2}$ is the axial frequency and $R_0^2 = \rho_0^2 + 2z_0^2$ is the physical dimension of the trap. We assume the product qU_0 to be always positive. The magnetic field $\mathbf{B} = B\widehat{\mathbf{z}}$ introduces the cyclotron frequency $w_c = qB/m$.

In this arrangement, the quadrupole potential acts as a trap only in one dimension, along the axis between the end-caps (we call this axis z), while the motion in the radial plane (x–y-plane) is unstable. The presence of the magnetic field along the z-axis provides trapping in the radial plane. For a complete description of the Penning trap configuration, see [11].

The Hamiltonian for a particle with the charge q and mass m in these fields is

$$\mathcal{H} = \frac{1}{2m}(P_x^2 + P_y^2 + P_z^2) - \frac{w_c}{2}(xP_y - yP_x) + \frac{m}{8}\left(w_c^2 - 2w_z^2\right)\left(x^2 + y^2\right) + \frac{m}{2}w_z^2 z^2. \tag{3}$$

From Hamiltonian (3) we get the *trapping condition*; that is to say, the factor $w_c^2 - 2w_z^2$ must be positive in order to obtain stable motion in the radial plane. Hereafter, we assume this condition. The dynamics arising from this system has been widely studied (see *e.g.* [13]), and its main feature is the harmonicity of the motion.

From the classical dynamics point of view, if we define $w^2 = (w_c^2 - 2w_z^2)/4$, the Hamiltonian (3) represents a three-dimensional harmonic oscillator of frequencies $w{:}w{:}w_z$ which is rotating around the z-axis with constant angular velocity $-w_c/2$. In particular, w_z is an "eigenfrequency" of the system and it governs the harmonic oscillation of the ion along the z-axis. However, the frequency w does not correspond to any of the two remaining eigenfrequencies of the system [13], the modified cyclotron frequency w_+ and the magnetron frequency w_-. The expressions of $w_\pm$ are

$$w_\pm = \frac{1}{2}(w_c \pm 2w).$$

In this sense, the ion trajectory is periodic only when the frequencies (w_+, w_z) become degenerate at $w_z = (2/3)w_c$ [13], which implies $w_c = 6w = (3/2)w_z$.

At this point, in order to clarify the role played by the frequencies w and w_z in the rest of the paper, we express (3) in cylindrical coordinates $(\rho, z, \phi, P_\rho, P_z, P_\phi)$ having

$$\mathcal{H} = \frac{1}{2m}(P_\rho^2 + P_z^2) - \frac{w_c}{2}P_\phi + \frac{P_\phi^2}{2m\rho^2} + \frac{m}{2}w^2\rho^2 + \frac{m}{2}w_z^2 z^2, \tag{4}$$

where P_ϕ is the conserved z-component of the canonical angular momentum. The corresponding six Hamilton equations of the motion are

$$\dot\rho = P_\rho, \qquad \dot z = P_z, \qquad \dot\phi = -\frac{w_c}{2} + \frac{P_\phi}{m\rho^2},$$
$$\dot P_\rho = -\frac{P_\phi^2}{m\rho^3} + w_c^2\rho, \qquad \dot P_z = w_z^2 z, \qquad \dot P_\phi = 0. \tag{5}$$

Let us suppose now that w and w_z are commensurable. In this case, any solution $\rho(t)$ and $z(t)$ corresponds to a periodic solution in the (ρ, z) plane – the *meridian plane* –. However, although $\dot\phi(t)$ will be also periodic with the same period T, we have for the polar angle ϕ

$$\phi(t) = -\frac{w_c}{2}t + \frac{P_\phi}{m}\int_0^t \frac{\mathrm{d}t}{\rho^2}\mathrm{d}t,$$
$$\phi(t+T) = \phi(t) + constant.$$

This angle indicates the position of the meridian plane, and it can be considered as the sum of two angles: one indicates the position of the ion in the orbit, and the other indicates the precession of the orbital plane. The precession of the orbital plane always exists, and in general, its frequency will not be resonant with the rotating frequency of the ion in the orbit. In other words, the existence of a periodic orbit in the plane (ρ, z) does not guarantee a periodic orbit in the three-dimensional space (x, y, z).

However, the precession of the orbital plane does not affect the periodicity of ρ and z, and this feature will be very useful to understand the dynamics when the ideal trap is perturbed.

Electrostatic perturbations may arise from imperfections in the physical design of the electrodes as well as from misalignments in the mounting. We model the electrostatic imperfections by means of the multipole expansion of the electrostatic potential [18]. This expansion, in spherical coordinates (r, θ, ϕ), takes the form

$$V = \sum_{l\geq 0} V_l, \qquad V_l = \sum_{k=0}^{l} a_{l,k}\, r^l\, \mathcal{P}_l^k(\cos\theta)\, \cos(k\,\phi), \quad (6)$$

$\mathcal{P}_l^k$ being the Legendre polynomials with $0 \leq k \leq l$. The first two terms are linear and give rise to constant forces. The next one is the *quadrupole* term V_2, which expressed in Cartesian coordinates is

$$V_2 = \frac{1}{2}a_{2,0}(2z^2 - x^2 - y^2) - 3a_{2,1}xz + 3a_{2,2}(x^2 - y^2), \quad (7)$$

where the first term on the right-hand corresponds to the perfect quadrupole potential appearing in (2). Since all terms in (7) are polynomials of second order, the motion remains harmonic. All higher orders in (6) will introduce nonlinearities in the motion.

In general, most of the terms in (6) can be made negligible by means of a careful design of the electrodes. For example, in a typical real Penning trap, the electrodes can be assumed to be cylindrically symmetric. Hence, all the terms in (6) with $k \neq 0$ vanish and we can write (6) as

$$V = V_2 + U_0 \sum_{l=3} a_l \left(\frac{r}{R_0}\right)^l \mathcal{P}_l^0(\cos\theta), \quad (8)$$

where we have dropped the constant term V_0 and where V_2 is the perfect quadrupole potential. With this model, the electrostatic perturbations depend on the actual geometry of the trap, because the coefficients $a_{l\geq 3}$ describe how far from the ideal configuration the electrodes are.

In this work, we consider the contribution of the first term in the expansion (8): the *sextupolar* term V_3,

$$V_3 = a_3 \frac{U_0}{R_0^3}(2z^2 - 3x^2 - 3y^2)z. \quad (9)$$

We remark that we can consider the presence of V_3 not only as an undesirable perturbation, but as a term we can intentionally introduce by means of a specific design of the electrodes different from the ideal one.

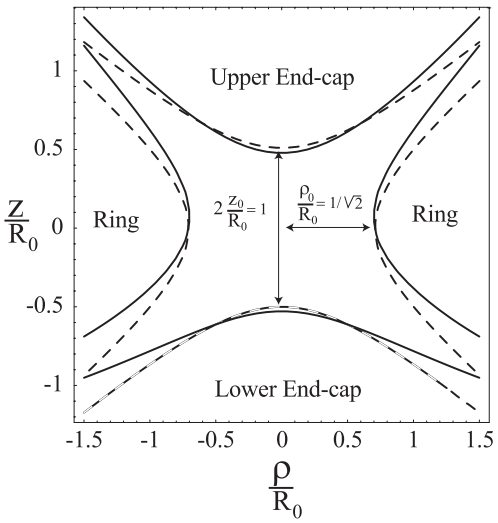

Fig. 1. Experimental realization of the sextupolar perturbed Penning trap. The dashed lines correspond to the electrodes in the ideal quadrupole configuration, while solid lines correspond to the electrodes deformed by the presence of a sextupolar perturbation ($a = 0.2$).

At this point, we express the complete electrostatic potential as

$$V = V_2 + V_3 = \frac{m w_z^2}{4q}\left[2z^2 - x^2 - y^2 + \frac{a_3}{R_0}\left(2z^2 - 3x^2 - 3y^2\right)z\right]. \quad (10)$$

In Figure 1 a typical electrode configuration is shown when a sextupolar contribution is added.

When the sextupolar perturbation is present, in cylindrical coordinates $(\rho, z, \phi, P_\rho, P_z, P_\phi)$, the Hamiltonian describing the system reads

$$\mathcal{H} = \frac{1}{2m}(P_\rho^2 + P_z^2) - \frac{w_c}{2}P_\phi + \frac{P_\phi^2}{2m\rho^2} + \frac{m}{8}(w_c^2 - 2w_z^2)\rho^2 + \frac{m}{2}w_z^2 z^2 + a_3\frac{m}{4}\frac{w_z^2}{R_0^3}(2z^2 - 3\rho^2)z. \quad (11)$$

Because the system is invariant under rotations around the z-axis (z-axially symmetric), P_ϕ is a constant of the motion, and Hamiltonian (11) represents a two-dimensional dynamical system. At a first glance, the dynamics arising from (11) depends on the parameters $(m, w_c, w_z, P_\phi, a, R_0)$ as well as on the energy $\mathcal{H}$. However, it is possible to reduce the number of parameters by means of the following procedure. First, we define the dimensionless time $\tau = w_c t$ and the dimensionless coordinates $\rho' = \rho/R_0$, $z' = z/R_0$. After applying these transformations to Hamiltonian (11) and after dropping primes in variables to simplify the notation, we get the following

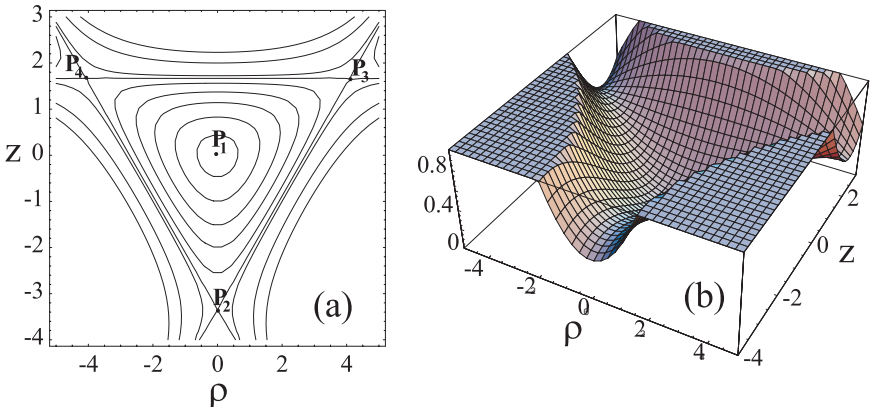

Fig. 2. (a) Equipotential curves of $U(\rho, z)$ and (b) potential energy surface $U(\rho, z)$ for $P_\phi = 0$. All figures for $a = 0.2$ and $\delta = 0.5$. Dimensionless units are used.

dimensionless Hamiltonian

$$\mathcal{H}' = \frac{\mathcal{H}}{mR_0^2 w_c^2} = \frac{1}{2}(P_\rho^2 + P_z^2) - \frac{1}{2}P_\phi + \frac{P_\phi^2}{2\rho^2} + \frac{1}{8}(1-2\delta^2)\rho^2 + \frac{1}{2}\delta^2 z^2 + \frac{1}{4}a\delta^2(2z^2 - 3\rho^2)z, \tag{12}$$

where we have defined $\delta = w_z/w_c < 1/\sqrt{2}$. Now the trapping condition reads as $\delta < 1/\sqrt{2}$. Hence, after this transformation, the number of parameters is reduced to (P_ϕ, δ, a) and the dimensionless energy $\mathcal{H}' = E$.

Note that the sextupolar term is controlled by two dimensionless parameters, on one side by a, that indicates the physical deformation of the electrodes, and on the other by δ, which modulates the effect of the deformation and determines the ratio between the axial and the cyclotron frequencies, *e.g.* the ratio between the electrostatic and the magnetic interactions.

At this point, we simplify the study by considering only the case $P_\phi = 0$. This situation can be easily achieved experimentally and is quite representative of the dynamics for all P_ϕ. For $P_\phi = 0$, the orbital plane (ρ, z) of the ion is not only rotating with angular velocity $-1/2$, *i.e.* $-w_c/2$ (see Eq. (5) for $P_\phi = 0$), but its orientation is always perpendicular to the $x-y$-plane. Taking this into account, the motion of the ion in the rotating orbital plane (ρ, z) is described by the Hamiltonian

$$\mathcal{H}' = \frac{1}{2}(P_\rho^2 + P_z^2) + \frac{1}{8}(1-2\delta^2)\rho^2 + \frac{1}{2}\delta^2 z^2 + \frac{1}{4}a\delta^2(2z^2 - 3\rho^2)z, \tag{13}$$

that formally represents a two-dimensional (ρ, z) harmonic oscillator of frequencies $w = w_c\sqrt{1-2\delta^2}/2$ – the radial frequency – and $w_z = w_c\delta$ – the axial frequency –. From the mathematical point of view, Hamiltonian (13) belongs to the so-called Hénon-Heiles family [19].

3 The potential energy surface

In order to know how the sextupolar perturbation modifies the perfect trapping, it is useful to study the shape of the effective potential $U(\rho, z)$ in (13),

$$U(\rho, z) = \frac{1}{8}(1-2\delta^2)\rho^2 + \frac{1}{2}\delta^2 z^2 + \frac{a\delta^2}{4}(2z^2 - 3\rho^2)z, \tag{14}$$

as the parameters δ and a vary. Now it is more illustrative to work in coordinates $(\pm\rho, z)$. It is easy to show that $U(\rho, z)$ has four critical points (see Figs. 2a and 2b): a minimum P_1, and three saddle points $P_{2,3,4}$. These critical points are

$$P_1 = (0,0), \qquad P_2 = \left(0, -\frac{2}{3a}\right),$$
$$P_{3,4} = \left(\pm\frac{1}{3a\delta^2}\sqrt{\frac{1-4\delta^4}{2}}, \frac{1-2\delta^2}{6a\delta^2}\right). \tag{15}$$

The three saddle points reduce to P_2 and P_3 when cylindrical coordinates (ρ, z) are used. We note that P_2 does not depend on δ. From expressions (15), we obtain the functions

$$D_2 = \frac{2}{3\,a}, \qquad D_{3,4} = \frac{\sqrt{3 - 4\,\delta^2 - 4\,\delta^4}}{6\,a\,\delta^2}, \tag{16}$$

where $D_{2,3,4}$ are the distances from the minimum P_1 – the center of the trap – to the saddle points $P_{2,3,4}$. When $\delta = \sqrt{3/10}$ we find that $D_2 = D_{3,4} = 2/3a$, *e.g.* the three saddle points are located at the same distance from the minimum P_1.

The energies of $P_{1,2,3,4}$ are

$$E_1 = 0, \qquad E_2 = \frac{2\delta^2}{27a^2}, \qquad E_{3,4} = \frac{(1-2\delta^2)^2(1+4\delta^2)}{432a^2\delta^4}, \tag{17}$$

and for $\delta = 1/2$ we find for the energies $E_2 = E_{3,4} = E_c = 1/54a^2$.

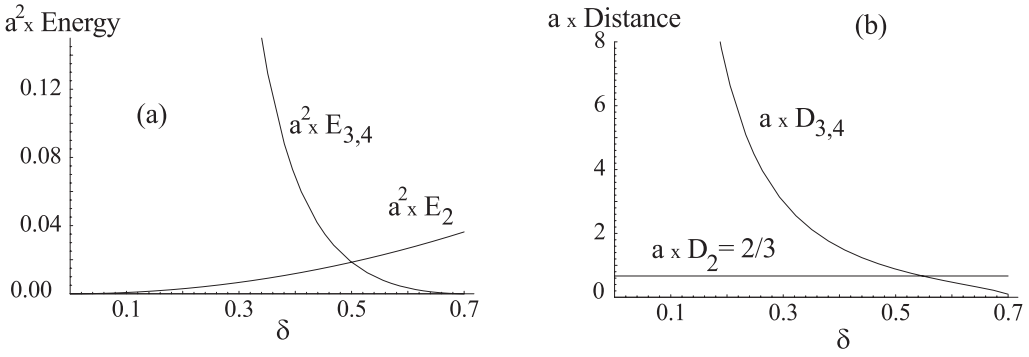

Fig. 3. (a) Evolution of the functions $a^2E_{2,3,4}$ as a function of δ. (b) Evolution of the functions $aD_{2,3,4}$ as a function of δ.

We note that expressions (16, 17) scaled with respect to $1/a$ and $1/a^2$, respectively: when a increases, the position of the saddle points shifts to the minimum P_1, while their corresponding energies $E_{2,3,4}$ decrease. As it was expected, when the deformation of the electrodes increases, the trapping energy interval and the zone where the ion can be trapped (the *trapping zone*) decrease.

To study the influence of δ on the energies and positions of the saddle points, it is convenient to plot the evolution of the functions $a^2E_{2,3,4}$ and $aD_{2,3,4}$ as a function of δ. These plots are shown in Figure 3. From Figure 3a we obtain that when δ increases, the energy E_2 increases while $E_{3,4}$ decreases, in such a way that when $\delta < 1/2$, $E_2 < E_{3,4}$ and for $\delta > 1/2$, $E_2 > E_{3,4}$. One more interesting feature arising from this figure is that E_2 shows a smoother evolution than $E_{3,4}$. Hence, while in the operating interval $0 < \delta < 1/\sqrt{2}$ the energy E_2 varies between $0 < E_2 < 1/27a^2$, the energy $E_{3,4}$ varies between $0 < E_{3,4} < \infty$. These energies are similar when $\delta \approx 1/2$.

When the position $D_{2,3,4}$ of the saddle points is analyzed, from Figure 3b we find a similar behavior. While the position of P_2 is constant with respect to δ, the positions of $P_{3,4}$ vary in the interval $0 < \delta < 1/\sqrt{2}$ between the values $0 < D_{3,4} < \infty$. These distances are similar when $\delta \approx \sqrt{3/10}$.

As a general conclusion, we can say that the effect of the perturbation is to create three channels of escape through which the ion is able to leave the trap. By fixing a, the position and energy of these channels – the saddle points – is actually controlled by the parameter δ. When δ is small, the axial frequency δ is smaller than the radial frequency $w = w_c\sqrt{1-2\delta^2}/2$ and the sextupolar perturbation is mainly affecting the motion in the z-direction. Hence, the energy of P_2 is much smaller than $E_{3,4}$ and it is located nearer to P_1 than $P_{3,4}$, so P_2 is the easiest channel to escape. When δ tends to $1/\sqrt{2}$, we find that the axial frequency is bigger than the radial frequency and the sextupolar perturbation mainly affects the motion in the ρ-direction. Thence, E_2 is much bigger than $E_{3,4}$ and $P_{3,4}$ are located nearer to P_1 than P_2 and so $P_{3,4}$ are the easiest channels to escape.

Moreover, the possibility of escape always exists because in the interval $0 < \delta < 1/\sqrt{2}$ at least one of the saddle points can have energy smaller than the energy of the ion. In this sense, for ion energies well below the crossing value $E_c = 1/54a^2$, Figure 3a suggests a safe zone to avoid escape centered around $\delta = 1/2$.

4 Phase space structure

In this section we focus on the study of the phase space governed by Hamiltonian (13). As it is well-known, the phase space structure is mainly characterized by the number and stability of the periodic orbits living in phase space [20]. When dealing with a system of two degrees of freedom, the computation of surfaces of section allows us to illustrate the phase space structure: in the regions of the phase space where the motion is regular, periodic orbits are clearly identified as fixed points of the Poincaré map. With this technique, we explore the evolution of the phase space as the parameters (E, δ, a) vary.

Firstly, we identify the values of the parameters (δ, a) for which periodic analytical solutions exist. The Hamilton equations of motion arising from (13) are

$$\begin{aligned} \dot{\rho} &= P_\rho, \quad \dot{P}_\rho = -\frac{1}{4}(1-2\delta^2)\rho + a\frac{3}{2}\delta^2\rho z, \\ \dot{z} &= P_z, \quad \dot{P}_z = -\frac{\delta^2}{4}(4z + 6az^2 - 3a\rho^2). \end{aligned} \tag{18}$$

In searching for particular solution of (18), we look for rectilinear solutions of the form $z = \alpha\rho$. By substituting in (18), we find the following solutions

- $\rho = 0$, which corresponds to a rectilinear orbit along the z-axis;
- $\alpha = \pm 1/2$ when $\delta = 1/\sqrt{6}$.

We recall that the rectilinear orbit along the z-axis always exists. However, the other two only exist for the special value $\delta = 1/\sqrt{6}$.

To look for additional periodic orbits, we compute the corresponding surface of section for $\delta = \sqrt{1/6}$. We define the surface of section as $\rho = 0$ and $P_\rho \geq 0$. Under these conditions, it appears as a region in the plane (z, P_z) bounded by the curves

$$P_z = \pm\sqrt{2E - \delta^2 z^2 - a\delta^2 z^3}. \tag{19}$$

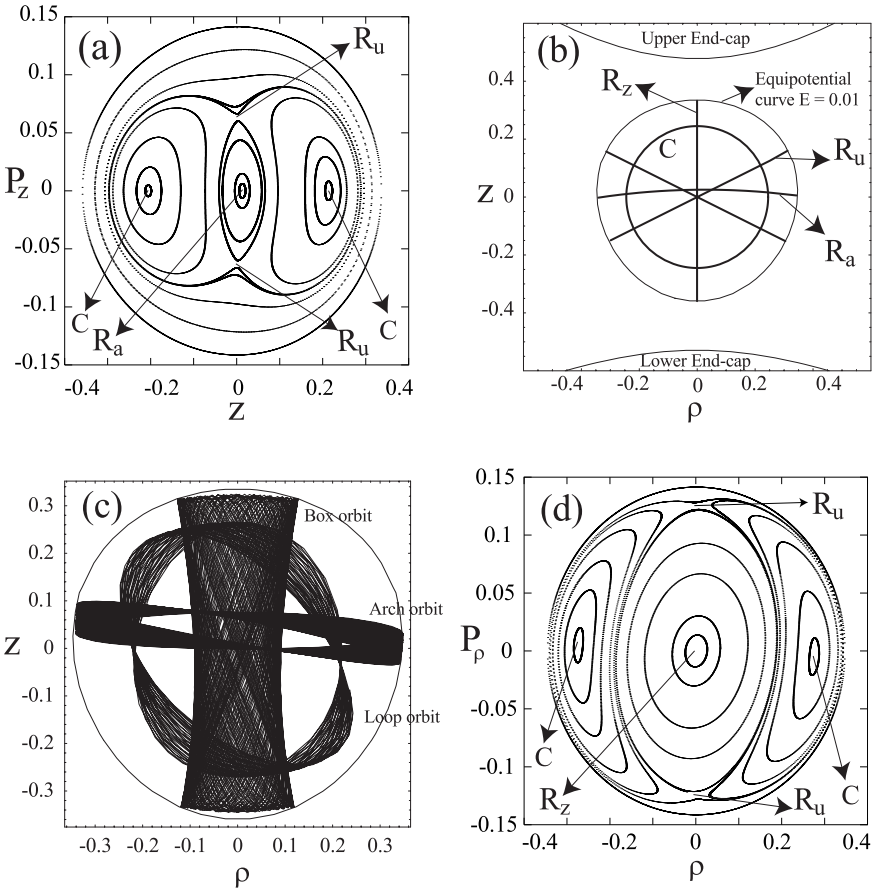

Fig. 4. (a) Surface of section ($\rho = 0, P_\rho \geq 0$). (b) Periodic orbits R_a, R_z, C and R_u. (c) Quasiperiodic orbits around R_z, R_a and C. Surface of section ($\rho = 0, P_\rho = 0$). All figures for $E = 0.01$, $a = 0.2$ and $\delta = 1/\sqrt{6}$.

It is worth noting that curves (19) correspond to the rectilinear orbit along the z-axis. Because we have to fix the the sextupolar parameter a and energy E, we take $a = 0.2$ and $E = 0.01$. For $a = 0.2$, the electrodes are quite deformed (see Fig. 1) and the energy $E = 0.01$ value is well below the crossing value $E_\mathrm{c} = 1/54a^2 = 0.462963$, and the escape is only possible outside the interval $0.073485 < \delta < 0.666756$. The mentioned surface of section (see Fig. 4a) presents four important structures.

(i) The stable (elliptic) fixed point located near the point $(0, 0)$ which corresponds to an *arch*-like orbit localized above the ρ-axis (see Fig. 4b). Note that this periodic orbit, named as R_a, does not cross the ρ-axis. We remark that R_a becomes a rectilinear orbit along the ρ-axis when the energy tends to zero. The levels around R_a correspond to quasiperiodic orbits with the same symmetry pattern as R_a. We call this kind of orbits *arch* orbits (see Fig. 4c).

(ii) The two stable fixed points C located near the axis ρ (see Fig. 4a). These fixed points correspond to almost circular orbits traveled in opposite sense (see Fig. 4b). These periodic orbits become circular orbits when the energy tends to zero, in such a way that they would be located at $(\pm\sqrt{6E}, 0)$. The levels around C correspond to quasiperiodic orbits with the same symmetry pattern. We call this kind of orbits *loop* orbits (see Fig. 4c).

(iii) The separatrix dividing these two regions of motion accumulates in the unstable (hyperbolic) fixed points symmetrically located at the point $(0, \pm\sqrt{2E/5} = \pm 0.063245)$. These hyperbolic points, named as R_u in Figure 4a, correspond to the rectilinear orbits $z = \pm 1/2\rho$ (see Fig. 4b).

(iv) Finally, taking into account that the limit of the surface of section is the rectilinear orbit along the z-axis – named R_z –, the levels above the separatrix correspond to quasiperiodic orbits with the same symmetry pattern, mainly localized along the z-axis. We call this kind of orbits *box* orbits [21] (see Fig. 4c). At this point, it is clear that the stability of R_z cannot be determined by looking at the surface of section, because this orbit appears as the limit of the section instead of a single point. However, if we compute the surface of section defined as $z = 0$ and $P_z \geq 0$, the periodic orbit R_z is the elliptic – stable – fixed point at $(0, 0)$ (see Fig. 4d), while R_a does not appear because it does not cross the ρ-axis. We use the surface of section ($\rho = 0, P_\rho \geq 0$) because with this definition we cover the entire phase space, while with the surface of section ($z = 0, P_z \geq 0$) the orbits that never cross the ρ-axis – *e.g.* R_a – are lost.

As it was expected when the energy is much smaller than the escape energies $E_{2,3,4}$, the phase space of the

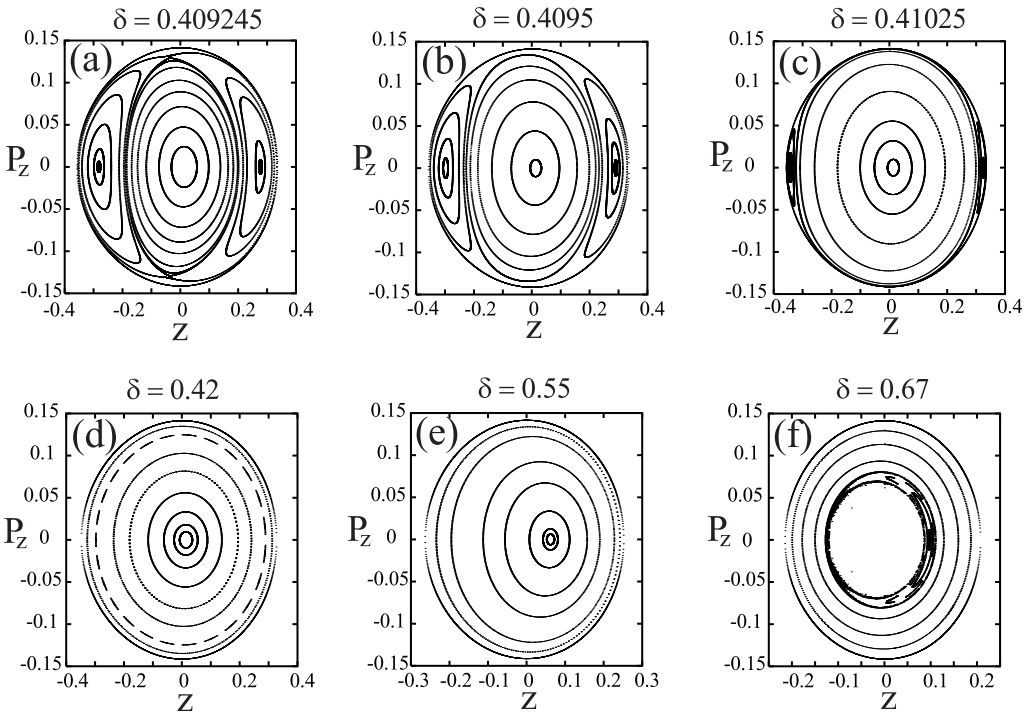

Fig. 5. Evolution of the surfaces of section ($\rho = 0, P_\rho \geq 0$) for $E = 0.01$, $a = 0.2$ as a function of δ.

system is regular and all the orbits are confined in adiabatic invariant tori.

When the parameter δ increases, the phase space suffers two consecutive changes that take place in the short interval $1/\sqrt{6} < \delta < 0.42$. These changes can be observed in the surfaces of section shown in Figures 5a to 5d. In this way, when $\delta \approx 0.42$, the phase space is made of rotations around $R_{\rm a}$. These rotations correspond to arch-like orbits when they are near $R_{\rm a}$, which become progressively box orbits as they go away from $R_{\rm a}$, that is to say, as they approach the limit of the surface of section – the orbit R_z –.

These changes can be perfectly understood in terms of two consecutive pitchfork bifurcations when the surfaces of section ($z = 0, P_z \geq 0$) are computed (see Fig. 6). In the first bifurcation, the two unstable orbits $R_{\rm u}$ and the stable orbit R_z come into coincidence, and, as a consequence, only R_z survives becoming unstable (see Figs. 6a and 6b). In the second bifurcation, the stable orbits C and the unstable orbit R_z collapse and only R_z survives, becoming stable again (see Figs. 6c and 6d).

When δ increases (see Fig. 5e for $\delta = 0.55$) the described phase space configuration remains almost the same. However, when $\delta < 0.666756$, the energy $E = 0.01$ is bigger than the energy $E_{3,4}$ of the saddle points $P_{3,4}$ (see Fig. 3a), and the ion is able to leave the trap through the saddles $P_{3,4}$. This fact can be observed in Figure 5f. This surface of section shows a gap in the central region which corresponds to the set of orbits which have initial conditions of escape. This gap is surrounded by a narrow stochastic layer inside which the fixed point $R_{\rm a}$ survives. Note that, even above the escape energy $E_{3,4}$, this surface of section shows a wide region of regular bounded orbits around R_z. These orbits correspond to orbits mainly oriented along the z-axis – box orbits –, that remain isolated from the channels of escape $P_{3,4}$. In this sense, when $\delta > 1/\sqrt{6}$, the arch orbits are the first that will be able to escape from the trap because they are more oriented along these channels than the box orbits.

Let us now to study the phase space evolution when $\delta < 1/\sqrt{6}$. This evolution can be observed in Figure 7. When $\delta = 0.4075$, the phase space structure has changed through a pitchfork bifurcation (compare Fig. 4a to Fig. 7a): the unstable fixed points $R_{\rm u}$ have disappeared, while $R_{\rm a}$ have became unstable. As a consequence, the phase space is filled with box orbits around R_z and loop orbits around C. When $\delta = 0.4$ a second pitchfork bifurcation takes place (see Fig. 7b): the stable fixed points C have disappeared while $R_{\rm a}$ becomes stable. Now, for $\delta < 0.4$, the surfaces of section are made of rotations around $R_{\rm a}$ (see Fig. 6c) which correspond to arch orbits when they are near $R_{\rm a}$, and to box orbits when they are near the limit of the surface of section – near R_z –. This phase space structure remains constant as δ decreases.

Finally, when $\delta < 0.073485$, the energy $E = 0.01$ is bigger than the energy E_2 of the saddle point P_2 (see Fig. 3a), and the ion is able to leave the trap through the saddle P_2. This fact can be observed in Figure 6d. We observe in that figure that the surface of section is not a bounded region because the rectilinear orbit R_z – which corresponds to the limit of the surface of section – is now an escape orbit. Note that Figure 7c shows an empty region which corresponds to the set of orbits with initial conditions of escape. Again, this empty region is surrounded by a very narrow stochastic layer. Moreover, the surface of section

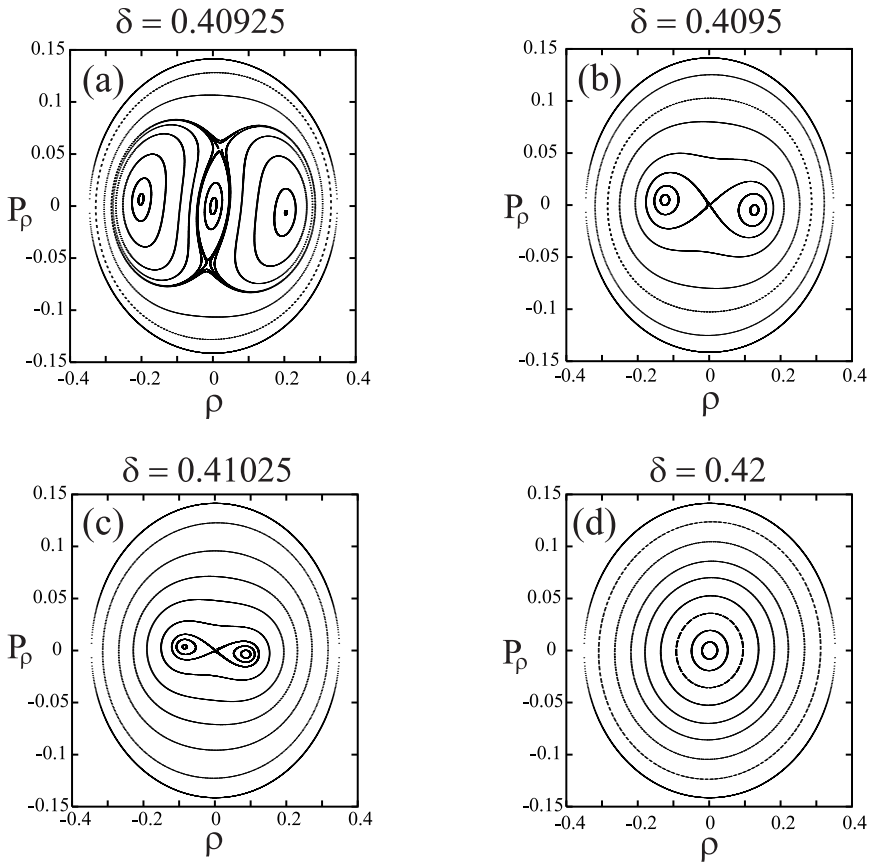

Fig. 6. Evolution of the surfaces of section ($z = 0, P_z \geq 0$) for $E = 0.01$, $a = 0.2$ as a function of δ. From (a) to (b) the first pitchfork bifurcation is observed, while between (c) and (d) the second one is observed. See the text for explanation.

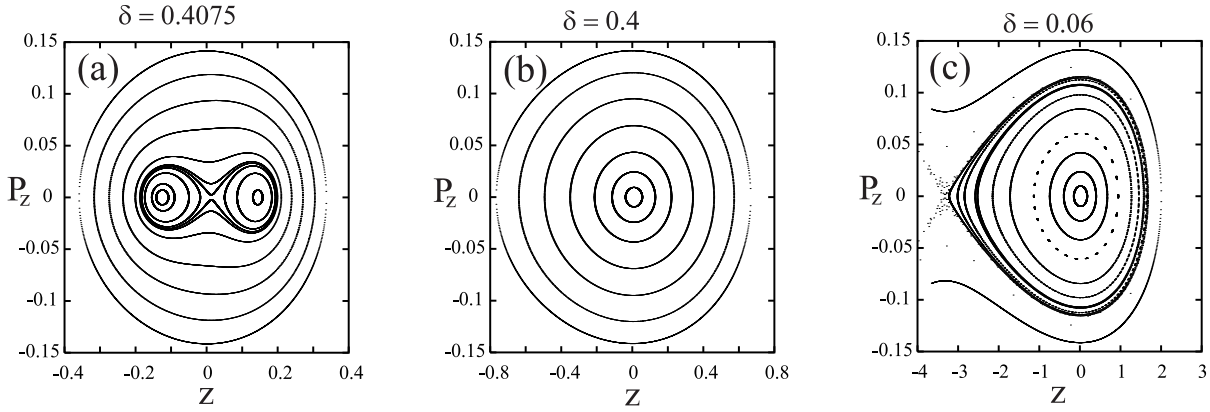

Fig. 7. Evolution of the surfaces of section ($\rho = 0, P_\rho \geq 0$) for $E = 0.01$, $a = 0.2$ as a function of δ. In (a) the first pitchfork bifurcation has occurred, while between (c) and (d) the second one is observed. See the text for explanation.

shows a wide region of regular bounded orbits around R_a. These orbits correspond to arch-like orbits that remain isolated from the channel of escape along P_2. Hence, when $\delta < 1/\sqrt{6}$, the box orbits are the first that will be able to escape from the trap because they have a better orientation along this channel than the arch orbits.

As a final remark, we have to take into account that in general not all the bounded orbits represented in the sequences of surfaces of section of Figures 4, 5, 6 and 7 have a physical meaning because, in addition to be bounded orbits, they must have a "size" smaller than the physical dimension of the trap. This fact can be understood by plotting the equipotential curve $U(\rho, z) = E$ for several values of δ. Such a plot is shown in Figure 8 for $E = 0.01$. We observe in that figure that, when δ is small, the equipotential curve spreads over a wide region of the z-axis. In this way, when δ tends to zero, most of the box orbits around R_z will be big to large in size, and therefore unphysical meaning,

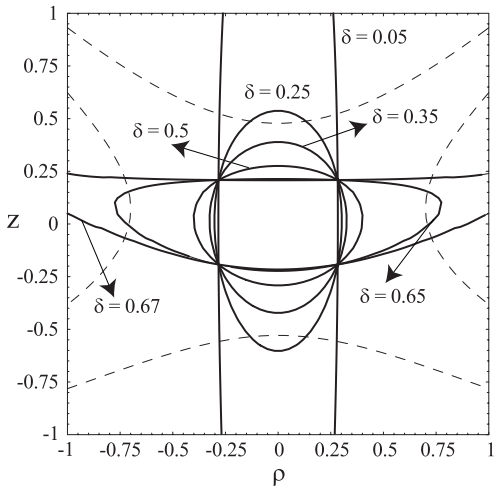

Fig. 8. Equipotential curves $U(\rho, z) = E = 0.01$, for $a = 0.2$ as a function of δ. The dashed curves are the electrodes.

while most of the arch orbits around R_a will have small size, being therefore real trapped orbits. When δ tends to $1/\sqrt{2}$, the equipotential curve mainly spreads over the ρ-axis and, thence, most of the arch orbits around R_a will have too much size to be physical, while most of the box orbits around R_z will be real trapped orbits.

A compensated behavior takes place for $\delta \approx 1/2$: the equipotential curve is well confined inside the trap, moreover the saddle points are located far away from the center of the trap and their energies are big and almost equal.

5 Conclusions

In the present work, we have studied the phase space (orbit) structure of a single ion in a realistic sextupolar perturbed Penning trap. In order to manage a two–dimensional Hamiltonian system, we assume that the perturbation is axial-symmetric. This assumption converts the z-component P_ϕ of the angular momentum into a constant of the motion, which can be treated as a common parameter. Besides the energy E and P_ϕ, two more parameters appear in the system: the parameter δ which indicates the ratio between the cyclotron and the axial frequencies, and the parameter a which indicates how far from the ideal quadrupolar configuration the electrodes are. We restrict our study to the case $P_\phi = 0$.

From the study of the effective potential of the problem, we find that the effect of the sextupolar parameter a is to create three channels of escape – saddle points – through which the ion is able to escape. The position and energy of these critical points are scaled with respect to a and in fact their energies and positions depend on the value of δ.

We find that three different families of orbits (arch, box and loop orbits) determine the structure of the phase space. Moreover, we show that the coexistence of these families depends on a very sensitive way on the parameter δ: when the system moves slightly away from the value $\delta = 1/\sqrt{6}$, the family of loop orbits disappears through two consecutive pitchfork bifurcations.

When δ tends to zero, we find that the box orbits are the first which are able to leave the trap, while when δ tends to $1/\sqrt{2}$, the arch orbits are the first to escape. We base the explanation of these facts on the shape of the potential energy surface as well as on the phase space structure.

It is worth noting that, although the rich dynamics we have studied arises from the presence of the sextupolar perturbation (parameter a), its effect on the ion motion is actually controlled by the parameter δ.

Although we have only considered in detail the axial-symmetric sextupolar perturbation, this paper provides a useful reference point to study the dynamics of trapped ions in more generally perturbed ion traps. In this sense, other axial-symmetric terms as the octupolar one [10], should be considered too. Moreover, a classical perturbative approach should be very useful in order to obtain a general geometric description of the perturbed ion motion. Work along these lines is now in progress [22].

This research has been partially supported by the Spanish Ministry of Education (DGES Proyect No. PB98-1576). The authors are specially indebted to one of the anonymous referees for his useful suggestions.

References

1. F.M. Penning, Physica **3**, 873 (1936); H. Dehmelt, Rev. Mod. Phys **62**, 525 (1990)
2. R. Blatt, P. Gill, R.C. Thompsom, J. Mod. Opt. **39**, 139 (1992)
3. J.N. Tan, J.J. Bollinger, B. Jelenkovic, D.J. Wineland, Phys. Rev. Lett. **75**, 4198 (1995); T.B. Mitchell, J.J. Bollinger, D.H.E. Dubin, X.-P. Huang, W.M. Itano, R.H. Baughman, Science **13**, 282, 1290 (1998); W.M. Itano, J.J. Bollinger, J.N. Tan, B. Jelenkovi, X.-P. Huang, D.J. Wineland, Science **30**, 279, 686 (1998)
4. S.L. Gilbert, J.J. Bollinger, D.J. Wineland, Phys. Rev. Lett. **60**, 2022 (1998)
5. J.I. Cirac, P. Zoller, Phys. Rev. Lett. **74**, 4091 (1995)
6. D.P. DiVicenzo, Science **270**, 255 (1995); C. Monroe, D.M. Meekhof, B.E. King, W.M. Itano, D.J. Wineland, Phys. Rev. Lett. **75**, 4714 (1995); Ch. Roos, Th. Zeiger, H. Rohde, H.C. Nägerl, J. Eschner, D. Leibfried, F. Schmidt-Kaler, R. Blatt, Phys. Rev. Lett. **83**, 4713 (1999); C.A. Sackett, D. Klelpinski, B.E. King, C. Langer, V. Meyer, C.J. Myatt, M. Rowe, Q.A. Turchette, W.M. Itano, D.J. Wineland, C. Monroe, Nature **404**, 256 (2000)
7. I. Marzoli, P. Tombesi, Europhys. Lett. **24**, 515 (1993)
8. R. Blatt, P. Gill, R.C. Thompson, J. Mod. Opt. **39**, 193 (1992); R.C. Thompson, Comm. At. Mol. Phys. **29**, 349 (1992); R.C. Thompson, Adv. At. Mol. Opt. Phys. **31**, 63 (1993); G.Zs.K. Horvath, R.C. Thompson, P.L. Knight, Contemp. Phys. **38**, 25 (1997); R.C. Thompson, Nathiagali Summer College, Pakistan, 1999
9. H. Walther, in *Irregular Atomic Systems and Quantum Chaos*, edited by J.-C. Gay (Gordon and Breach Science Publishers, 1992); M. Moore, R. Blümel, Phys. Rev. A **48**,

3082 (1993); D. Farrelly, J.E. Howard, Phys. Rev A **49**, 1494 (1994)
10. D.J. Bate, Ph.D. thesis, Imperial College, London, 1991; D.J. Bate, K. Dholakia, R.C. Thompson, D.C. Wilson, J. Mod. Opt. **39**, 305 (1992)
11. P.K. Ghost, *Ion Traps* (Oxford Univ. Press, New York, 1995)
12. M. Kretzschmar, Phys. Scripta **46**, 544 (1992)
13. G.Zs.K. Horvath, J.L. Hernandez-Pozos, K. Dholakia, J. Rink, D.M. Segal, R.C. Thompson, Phys. Rev. A **57**, 1944 (1998)
14. T. Bergeman, Bull. Am. Phys. Soc. **31**, 939 (1986); T. Bergeman, private communication; H.J. Metcalf, P. van der Straten, *Laser coolong and trapping* (Springer, New York, 1999)
15. H. Friedrich, D. Wintgen, Phys. Rep. **183**, 37 (1989); J.P. Salas, A. Deprit, S. Ferrer, V. Lanchares, J. Palacián, Phys. Lett. A **242**, 83 (1998); J.P. Salas, V. Lanchares, Phys. Rev. A **58**, 434 (1998)
16. E. Backhaus, J. Fajans, J. Wurtele, Phys. Plasmas **6**, 19 (1999)
17. T.M. Squires, P. Yesley, G. Grabielse, Phys. Rev. Lett. **86**, 5266 (2001)
18. J.D. Jackson, *Classical Electrodynamcis* (Wiley, New York, 1975)
19. S. Ferrer, M. Lara, J. Palacián, J.F. San Juan, A. Viartola, P. Yanguas, Int. J. Bif. Chaos **8**, 1199 (1998); S. Ferrer, M. Lara, J. Palacián, J.F. San Juan, A. Viartola, P. Yanguas, Int. J. Bif. Chaos **8**, 1215 (1998)
20. M.C. Gutzwiller, *Chaos in Classical and Quantum Mechanics* (Springer Verlag, New York, 1990), 1 IAM
21. The names *box* and *loop* were coined by J. Binney, S. Tremaine, *Galactic Dynamics* (Princeton University Press, Princeton, New Jersey, 1989)
22. V. Lanchares, A.I. Pascual, J. Palacián, P. Yanguas, J.P. Salas, Chaos **12**, 87 (2002)